ISSN 1070-3632, Russian Journal of General Chemistry, 2013, Vol. 83, No. 11, pp. 2148–2158. © Pleiades Publishing, Ltd., 2013.
Original Russian Text © A.B. Rinkevich, A.M. Burkhanov, M.I. Samoilovich, A.F. Belyanin, S.M. Kleshcheva, E.A. Kuznetsov, 2012, published in Rossiiskii Khimicheskii Zhurnal, 2012, Vol. 56, Nos. 1–2, pp. 26–35.

Three-Dimensional Nanocomposite Metal Dielectric Materials on the Basis of Opal Matrices

A. B. Rinkevich[a], A. M. Burkhanov[a], M. I. Samoilovich[b], A. F. Belyanin[b], S. M. Kleshcheva[b], and E. A. Kuznetsov[c]

[a] *Institute of Metal Physics, Ural Branch, Russian Academy of Sciences, ul. Sofii Kovalevskoi 18, Yekaterinburg, 620219 Russia*
e-mail: rin@imp.uran.ru

[b] *Tekhnomash Central Research Technological Institute OAO, ul. Ivana Franko 4, Moscow, 121108 Russia*
e-mail: samoylovich@technomash.ru

[c] *Nizhny Tagil State Social Pedagogical Academy, Krasnogvardeiskaya ul. 57, Nizhny Tagil, 622331 Russia*

Received June 1, 2012

Abstract—The microwave properties of 3D nanocomposites based on opal matrices containing one or two transition metal particles have been investigated. Phase analysis of the nanocomposites has been carried out. Magnetic field dependences of transmission and reflection coefficients were obtained. Magnetic resonance and antiresonance spectra have been reconstructed. Frequency dependences of resonance and antiresonance amplitude have been obtained. It has been found that the magnetic resonance amplitude of a nanocomposite containing particles of two metals is essentially higher than that of a nanocomposite with particles of one metal.

DOI: 10.1134/S1070363213110340

Literature Review on Nanocomposite Materials on the Basis of Opal Matrices

Opal-based photonic crystals are actual objects for research on electromagnetic properties in the microwave (MW) range. Of interest are both basic issues associated with such crystals and their practical application [1]. Most researchers' attention is focused on the optical and MW properties of opal matrices in view of possible interactions of their subsystems [2]. Both electromagnetic transmission and reflection properties of photonic crystals are being studied.

In theoretical description of the observed phenomena, photonic crystals are considered as an ensemble of microspheres [3–6]. The physical properties and structure of opal matrices with embedded metal and ferromagnetic nanoparticles were studied in detail in [7, 8]. Much interest is attached to theoretical and experimental research on the propagation of electromagnetic waves in media with negative refractive indices [6]. The problem of wave penetration though a plate of such material with demonstration of the focusing effect is considered as a classical one. This problem arises in the calculation and design of antennas [9].

At present a detailed study in given to the linear and nonlinear properties of opal matrices, which are manifested in their ability to transmit a powerful coherent radiation [2]. Specific features of the optical properties of 2D and 3D objects on the basis of opal matrices were studied [10]. Embedding magnetic or metal materials into intersphere voids of opal matrices opens up wide perspectives for application of opal metrices as magnetic metamaterials in super-high-frequency (SHF) nanoelectronic devices.

Microwave methods seem to be especially efficient for research on nanocomposites, since they make possible fairly facile estimation of dynamic and relaxation parameters of such materials. Using elements of SHF technics and different measurement schemes, one can realize different mutual orientations of MW fields and an external magnetic field and thus ensure the most efficient interaction of embedded nanoparticles with magnetic fields. Opal matrices with embedded magnetic metal nanoparticles can be classed with materials suitable for creation of media with a negative refractive index. So-called left-handed media with a negative actual magnetic permeability can be first of all created in the range of magnetic resonances. In the

magnetic resonance range, the dynamic magnetic permeability changes sign and may strongly vary in value. The interaction of SHF magnetic fields with magneto-photonic crystals considered as metamaterials is an actual field of research of metal-containing opal-based nanocomposites, which opens new perspectives of application for the material resonance phenomenon [11, 12].

A special class of metamaterials includes media with a near-zero permittivity, so-called epsilon-near-zero (ENZ) media. The supercoupling effect is a glowing example of anomalous propagation of electromagnetic waves in such media [13, 14]. This phenomenon consists in wave tunneling through narrow channels and bends joining two waveguides, under conditions when normal wave propagation is impossible. A theoretical consideration of the propagation of electromagnetic waves in ENZ media is given in [15]; therewith, the continuous-wave regime and transition processes are discussed.

To study resonance magnetization dynamics and magnetic relaxation of small particles is of importance for understanding high-frequency phenomena in metamaterials. The magnetic relaxation processes in ensembles of iron nanocrystals were studied by Buchanan et al. [16]. Moiseev et al. [17] studied scattering properties of media containing metal inclusions in the shell. The authors made use of the Maxwell–Garnett model to study the complex efficient refractive index of a matrix metal-dielectric composite medium with spheroid-shaped silver inclusions.

The application of 3D opal-based nanocomposites in controlled MW electronic devices requires knowledge of a number of such parameters as electromagnetic wave decay and magnetic resonance amplitude, spectrum, and linewidth. The resonance field and width and shape of the resonance line depend on nanoparticle size [18].

The MW properties of 3D opal-based nanocomposites are associated with their phase composition and magnetic state. The magnetic properties of nanoparticles are much different from those of bulk materials. Nanoparticle surface contributes much into the magnetic anisotropy of nanocomposites; and an important role in the latter also belongs to superparamagnetic relaxation [19, 20]. The magnetic state of nanocomposites is a factor responsible for their MW behavior in magnetic field, in particular, resonance phenomena.

In the present work we have studied the electromagnetic properties of 3D opal-based nanocomposites having transition metal (nickel, iron, cobalt) nanoparticles embedded into intersphere voids.

Synthesis, Chemical Composition, and Structure of Metal Nanocomposites

The synthesis of opal matrices with SiO_2 spheres 200–350 nm in diameter has been described in a number of works (cf., for example, [7, 21]). In the present work, the opal matrices with SiO_2 spheres 280 nm in diameter were synthesized by the following technology. The orthosilicic acid ester $Si(OC_2H_5)_4$ was hydrolyzed in an ethanol solution in the presence of ammonium hydroxide as a catalyst to obtain amorphous SiO_2 as fine branched nanoparticles. By polycondensation the latter were converted into spherical amorphous SiO_2 particles. After settling of the suspension, a hydrogel with the liquid content of up to 50–60 wt % precipitated. Provided no precautions were taken, a chalk-like and fragile material formed after drying. For strengthening and complete removal of water, dry opal matrices were subjected to thermal treatment.

The most simple and common method of synthesis of metal-containing opal-based nanocomposites involves impregnation of the matrix with a precursor and subsequent thermal treatment which forms particles with a desired chemical composition in intersphere voids of the opal matrix. Precursors should be readily soluble in water and transform into oxides at moderate temperatures, lest be destroyed on thermal treatment.

In the present work we used soluble metal nitrates as precursors. The impregnation procedure was repeated many times (up to 20) to ensure gradual filling of the intersphere space of opal matrices. On the subsequent thermal treatment at 500–700°C nitrate groups are partially destroyed and unstructured water is completely removed.

Before nanoparticles had been embedded into intersphere voids, the opal matrix had a periodic structure of densely packed submicron silicate spheres. This structure was established by X-ray phase analysis and electron microscopy. The particles embedded into intersphere voids by impregnation followed by drying consist of metal oxides. To obtain a nanocomposite containing metal particles, the samples were annealed under hydrogen at 600–700°C. The following annealing protocol was used:

Table 1. Elemental composition of a nanocomposite embedded with iron and nickel nanoparticles

Element	wt %
O	32.78
Si	44.32
Fe	04.65
Ni	18.25

(1) air pumping;

(2) heating for desorption of volatiles from the sample (starts at 100–200°C and completes at 600°C);

(3) raising the hydrogen pressure to 2.5 atm after desorption completion;

(4) annealing for 7 h at 600–700°C; the hydrogen pressure the most actively decreases within the first hour.

Table 1 presents as an example the elemental analyses of a nickel and an iron-containing nanocomposite annealed under hydrogen. The analysis was performed by energy dispersive X-ray spectroscopy (EDAX). Figure 1a shows an image of the structure of the nanocomposite with embedded cobalt nanoparticles, obtained on a Quanta-200 scanning electron microscope. The embedded particles have irregular shapes and are 10–80 nm in size.

As seen from Fig. 1, the embedded substance partially encapsulates the submicron SiO_2 spheres and also is present in the intersphere space; its concentration is 5–15 vol %. X-ray phase analysis of a DRON-6 diffractometer showed that the particles comprise cobalt metal (94.8%) and cobalt oxide CoO (5.2%). Figure 1b shows the structure of the nanocomposite containing particles of two metals: nickel and iron.

The synthesized samples were found to have the following compositions: $Co_{0.5}Ni_{0.5}$, $Ni_{0.6}Fe_{0.4}$, $Ni_{0.75}Fe_{0.2}Co_{0.05}$.

Magnetic and Electrical Properties of Nanocomposites

Magnetic measurements were performed on a Quantum Design MPMS-XL magnetometer (field intensity up to 50 kOe, temperature range 2–300 K). Magnetization curves and hysteresis loops, as well as temperature dependence of magnetic moment at the field intensity of 10 kOe were measured. Special attention in the present work was focused on the electromagnetic wave frequencies and magnetic field intensities corresponding to magnetic resonance conditions. Therefore, of the highest interest is the magnetization curve of nanocomposites, since this is magnetization that determines the magnetic resonance field. Figure 2 shows the dependence of the magnetic moment of the cobalt-embedded nanocomposite on the magnetic field intensity at room temperature. In the field intensity range up to 50 kOe, this dependence is close to directly proportional and shows no saturation signs.

Electrical characteristics of metal-embedded nanocomposites were measured. Since the contents of metal nanoparticles in the nanocomposites are no more than 15%, which is lower than the percolation threshold, their specific *dc* electrical conductivity is quite high. The specific electrical conductivity of the cobalt-embedded nanocomposite ρ is higher than 2.5×10^7 Ω cm. In [21] we estimated for the same sample the dielectric

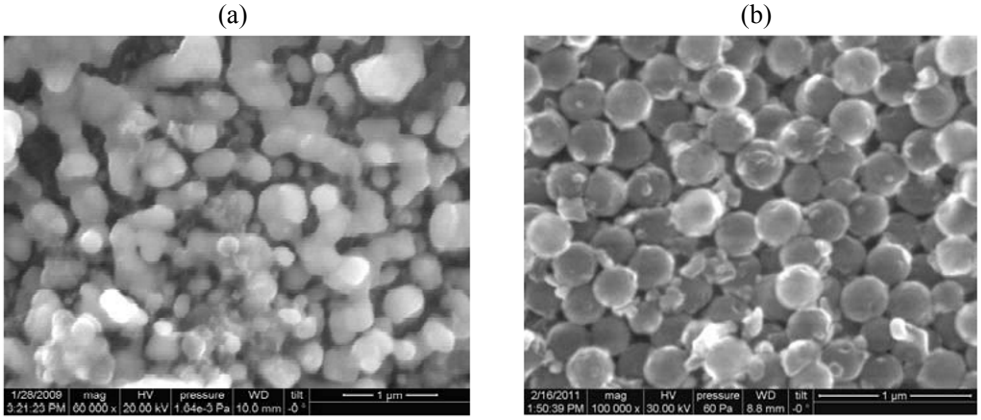

Fig. 1. Electron microscope image of the structure of an opal-based nanocomposite embedded with (a) cobalt (×60000, 20 kV) and (b) nickel/cobalt (×100000, 30 kV) particles.

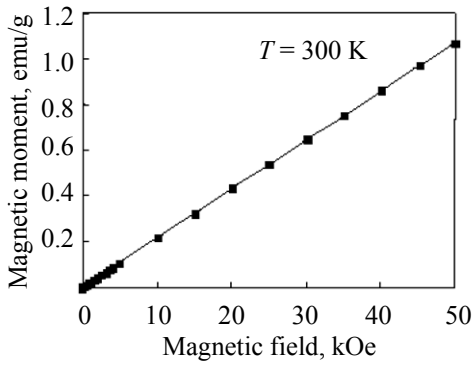

Fig. 2. Magnetization curve of the cobalt-embedded nanocomposite.

constant ε and conductivity σ in the millimeter frequency range. In the range 26–38 GHz, σ = 0.36 S/m. The complex dielectric constant of the nanocomposite has two components: real (ε') and imaginary (ε") which depends on the angular frequency ω of incident wave:

$$\dot{\varepsilon} = \varepsilon' - \varepsilon'' = \varepsilon - i\frac{\sigma}{\omega\varepsilon_0},$$

where ε' = 3.3.

The ε"/ε' ratio is 0.06. The SHF conductivity of the nanocomposite is much higher than the *dc* conductivity.

Phase Composition of Nanocomposites

Phase analysis of nanocomposites with metal nanoparticles embedded into intersphere voids of opal matrices was performed both before and after annealing of the samples under hydrogen. The X-ray diffraction patterns of the samples, obtained on a DRON-3M diffractometer, are shown in Fig. 3.

The following phases were identified in nanovoids:

– Ni,Co-embedded nanocomposite obtained after nine impregnation cycles and annealed at 725°C: NiO, cubic syngony, space group *Fm*3*m* (78-0643) and Co_3O_4, cubic syngony, space group *Fd*3*m* (80-1533);

– Fe,Ni-embedded nanocomposite obtained by the same procedure: $FeNi_3$, cubic syngony, space group *Pm*3*m* (38-0419);

– Ni,Co,Fe-embedded composite obtained after nine impregnation cycles and annealed at 700°C: Ni, cubic syngony, space group *Fm*3*m* (04-0850); Co, cubic syngony, space group *Fm*3*m* (15-0806) and, probably, $FeNi_3$, cubic syngony, space group *Pm*3*m* (38-0419);

– Pd,Co-embedded nanocomposite obtained after seven impregnation cycles and annealed at 700°C: Pd, cubic syngony, *Fm*3m (87-0645) and Co, hexagonal syngony, space group $P6_3/mmc$ (89-7373).

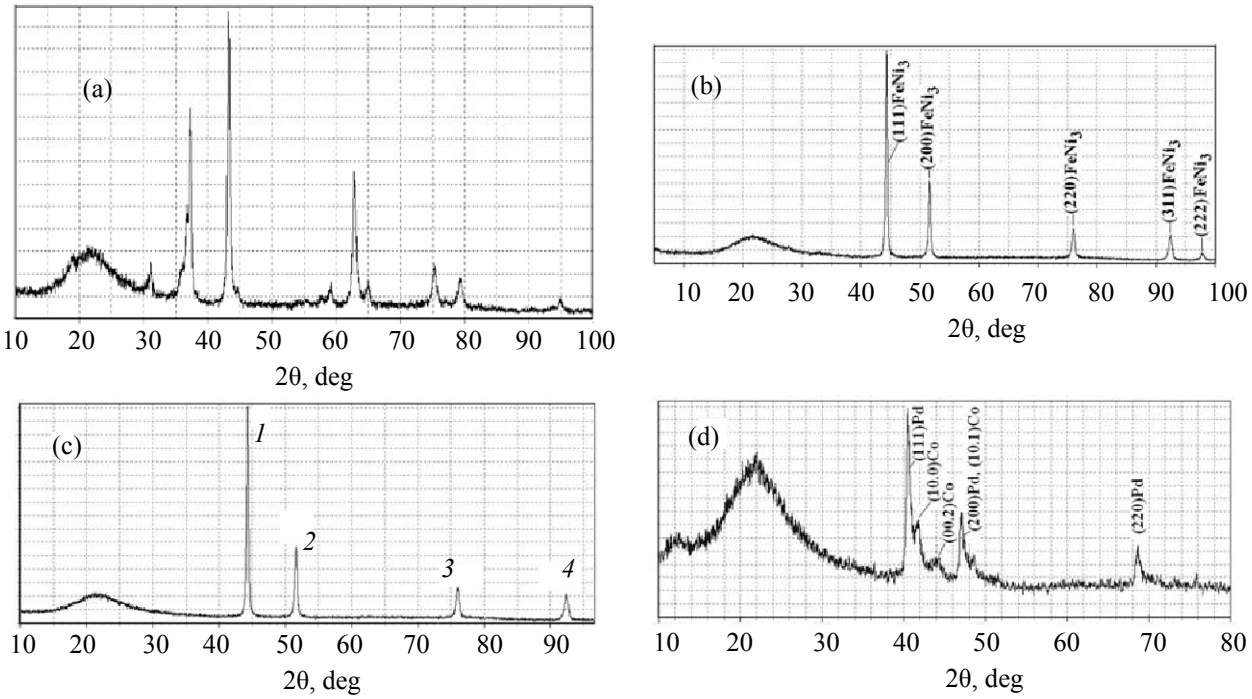

Fig. 3. X-ray diffraction patterns of opal-based nanocomposites embedded with (a) Ni and Co, (b) Fe and Ni, (c) Ni, Co, and Fe; and (d) Pd and Co particles.

Table 2. X-ray diffraction data (CuK_α radiation) of opal matrices with metal particles in intersphere voids

Bragg angle, 2θ, deg	Peak half-width, deg	*hkl*	CSR size[a], nm
Sample in Fig. 3a initial			
NiO, cubic syngony, *Fm*3*m*			
37.252	0.409	111	22.8
43.232	0.416	200	22.8
62.757	0.514	220	20.1
Co_3O_4, cubic syngony, *Fd*3*m*			
31.203	0.290	220	31.6
36.669	0.409	311	22.8
annealed in hydrogen			
Ni, cubic syngony, *Fm*3*m*; Co, cubic syngony, *Fm*3*m* (reflections do not overlap)			
44.461	0.345	111	27.7
51.813	0.462	200	21.3
76.198	0.466	220	24.1
Sample in Fig. 3b annealed in hydrogen			
$FeNi_3$, cubic syngony, *Pm*3*m*			
44.149	0.394	111	24.2
51.411	0.473	200	20.7
75.615	0.519	220	21.5
Sample in Fig. 3c annealed in hydrogen Ni, cubic syngony, *Fm*3*m* Co, cubic syngony, *Fm*3*m* $FeNi_3$, cubic syngony, *Pm*3*m* (reflections do not overlap)			
44.298	0.302	111	31.6
51.619	0.341	200	28.8
75.963	0.405	220	27.7

[a] (CSR) Coherent scattering region.

The X-ray diffraction characteristics of some samples are listed in Table 2. The crystallite dimensions along the directions perpendicular to the {*hkl*} axes were determined by the broadening (half width of the diffraction maximum) of the (*hkl*) reflection: $L = k\lambda/\beta\cos\theta_{hkl}$, where k is a constant; λ, X-ray radiation wavelength; β, reflection broadening; and θ_{hkl}, reflection diffraction angle.

The size of crystallites in unannealed and hydrogen-annealed nanocomposite samples spans the range 20.1–31.6 nm. In all the synthesized nanocomposites, crystallites have the shape of equiaxial grains, and only Co_3O_4 crystallites are slightly stretched along the crystallographic axis <110>. Hydrogen annealing slightly enlarges the coherent scattering region.

Thus, the intersphere nanovoids in opal-based metal-embedded nanocomposites contain, depending on thermal treatment conditions, the following phases: NiO (cubic syngony, space group *Fm*3*m*); Co_3O_4 (cubic syngony, space group *Fd*3*m*); Ni (cubic syngony, space group *Fm*3*m*); Co (cubic syngony, space group *Fm*3*m*); $FeNi_3$ (cubic syngony, space group *Pm*3*m*); Co (cubic syngony, space group *Fm*3*m*); and Co (hexagonal syngony, space group e*P*63/*mmc*).

Microwave Measurements

Mocrowave measurements were performed in the frequency range 26–38 GHz, using standard waveguides operating at the dominant mode H_{10}. Single-mode regime was used over the entire frequency range. A sample was placed into a waveguide with the cross-section 7.2×3.4 mm^2 (Fig. 4). The sample was arranged transversally to the SHF tract. The external constant magnetic field H, created by an electromagnet, was applied perpendicularly to the wave vector q. The external magnetic field is either coaxial/parallel or perpendicular to the plane of the MW magnetic field vectors $H_{\perp}$. Measurements were performed at room temperature.

Transmission and reflection coefficient modules (D and R, respectively) and their relative changes in the external magnetic field were measured: $d_m = [|D(H)| - |D(0)|]/|D(0)|$, where $|D(H)|$ is the transmission coefficient module in the magnetic field H and $r_m = [|R(H)| - |R(0)|]/|R(0)|$, where $|R(H)|$ is the reflection coefficient module. (For the sake of brevity, in what follows by the transmission and reflection coefficients we mean their modules).

Below we present the results of measurements of field dependences of transmission and reflection coefficients for certain opal-based composite materials. First of all, of interest are the changes in the coefficients of resonant frequencies, induced by magnetic resonance and antiresonance. The magnetic resonance absorption of electromagnetic wave generally leads to a minimum on the field dependence of reflection and

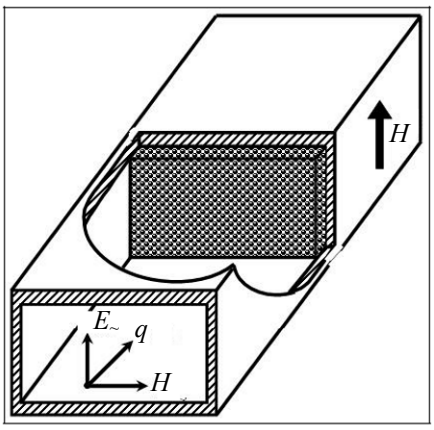

Fig. 4. Sample arrangement in the waveguide in microwave measurements.

transmission coefficients. The magnetic antiresonance produced by a change of the sign of magnetic permeability of a metallic ferromagnetic in fields lower than the field of the uniform magnetic resonance mode, can slightly increase either transmission or reflection coefficient, or both coefficients [21].

For a uniform resonance mode to be observed, the material should be ferro- or ferrimagnetic. Therefore, after metal oxide particles had been embedded into intersphere nanovoids of the opal matrix, the material was necessary to anneal under hydrogen. During annealing metals reduced from their oxides to form a metal–dielectric nanocomposite. For a magnetically ordered nanocomposite, it is imperative that at least one of the metals be transition or rare-earth.

In the field dependences of nanocomposites with embedded oxide particles, no resonance changes should be expected in the studied ranges of frequencies and fields. Thus, no resonance changes were observed on the field dependence of transmission coefficient for the nanocomposite containing antiferromagnetic CoO particles, and all changes were less than 1%.

As to hydrogen-annealed nanocomposites with one transition metal particles, the field dependence of MW reflection coefficient for the nickel-embedded nanocomposite shows antiresonance maxima in the range 3–5 kOe and magnetic resonance at 8–10 kOe (Fig. 5a). The signal changes induced by both antiresonance and resonance are fairly strong and reach 60%. The curve for the transmission coefficient of the same nanocomposite (Fig. 5b) shows changes associated with magnetic resonance only, while antiresonance is not observed. This circumstance differentiates metal-

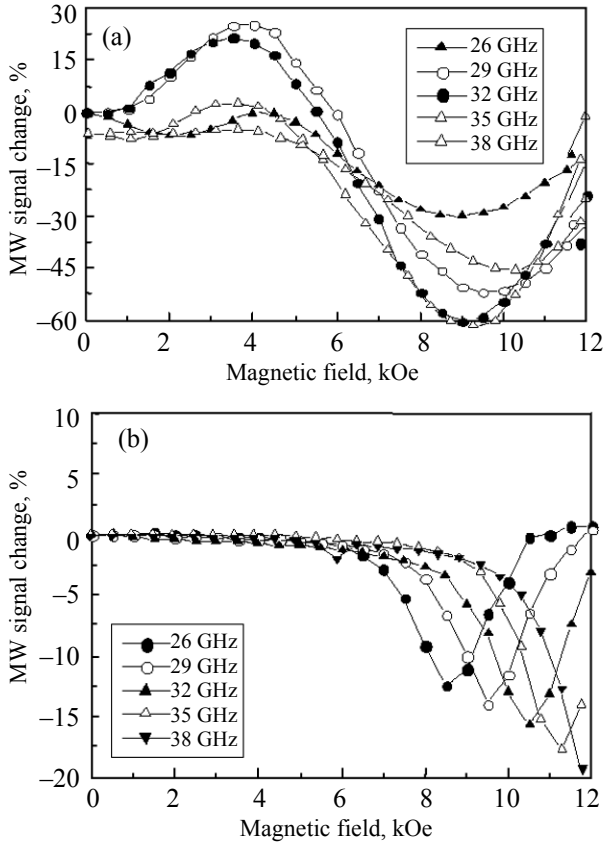

Fig. 5. Field dependence of the (a) reflection and (b) transmission coefficients for the nickel-embedded nanocomposite.

embedded nanocomposites from previously studied dielectric nanocomposites containing ferrite spinels [22]. There is a regularity theoretically established for magnetic dielectric nanocomposites: If the coefficients change only slightly, then their field-induced changes are similar to each other, but the transmission coefficient changes slightly greater than the reflection coefficient. Experimental evidence for this regularity was obtained for nanocomposites containing various ferrites. Comparison of Figs. 5a and 5b suggests that metal–dielectric composites may not adhere to this regularity. For the 3D nanocomposite containing nickel and cobalt particles, antiresonance is seen in the curves both for reflection and transmission coefficients (Fig. 6).

The nanocomposite embedded with iron and nickel particles showed no antiresonance in wave transmission, whereas magnetic resonance is clearly observed, and, moreover, it has a large amplitude. The field dependence of reflection coefficient shows both resonance and, at certain frequencies, antiresonance.

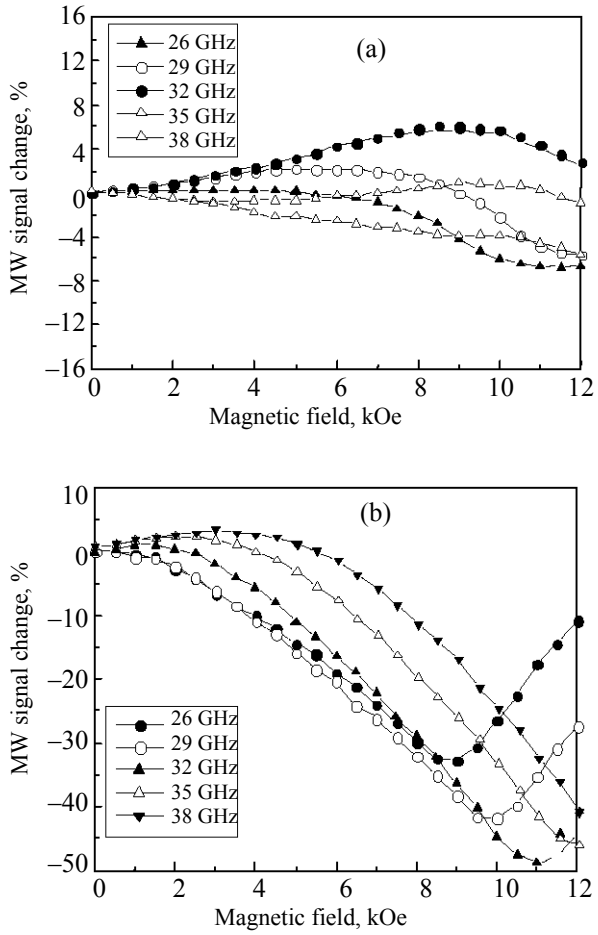

Fig. 6. Field dependence of the (a) reflection and (b) transmission coefficients for the nickel-and-cobalt-embedded nanocomposite.

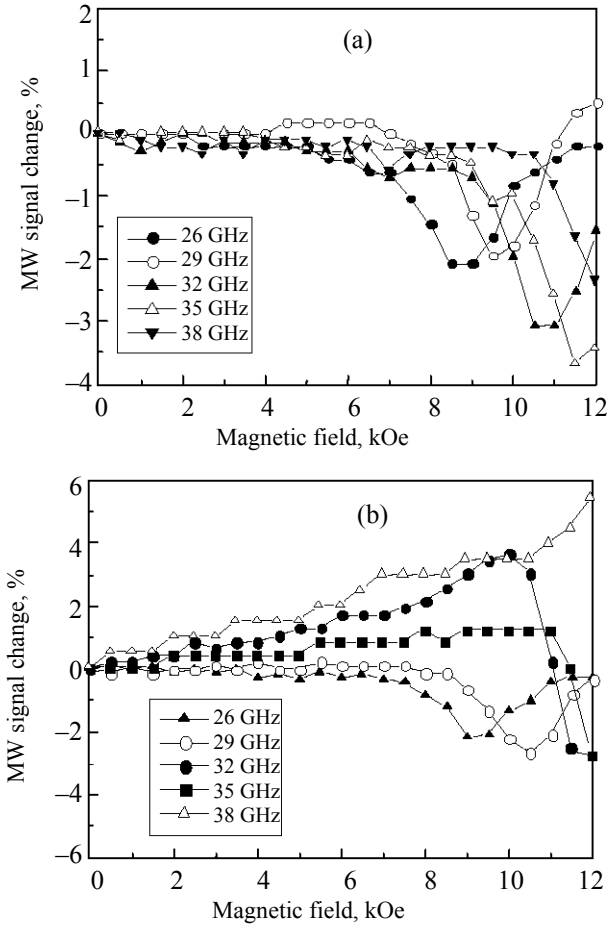

Fig. 7. Field dependence of the (a) reflection and (b) transmission coefficients for the neodyminum-and-iron-embedded nanocomposite.

Let us now focus on the resonance phenomena in the nanocomposite containing both a transition and a rare-earth metal particles. The field dependences of the reflection and transmission coefficients of the neodymium-and-iron-embedded nanocomposite (Fig. 7) contain a broad magnetic resonance band, which points to a strong magnetic inhomogeneity. The resonance amplitude is not so large, much smaller than in the composite containing two transition metals. No antiresonance was observed.

Magnetic Resonance and Antiresonance Spectra

The experimental dependences of the transmission and reflection coefficients on the magnetic field strength, measured at various frequencies, allow reconstruction of magnetic resonance and antiresonance spectra. Let us assume that the resonance and antiresonance positions coincide with, respectively, a minimum and a maximum on the field dependence of one or the other coefficient.

Figure 8 shows the magnetic resonance and antiresonance spectra obtained for two samples of a cobalt-embedded nanocomposite. As would be expected, at the same frequency, magnetic resonance is observed in a higher field than antiresonance. The magnetic resonance spectrum of sample no. 130/7 looks unusually: At frequencies lower than 32 GHz it strongly deviates from linearity, implying that the magnetization curve of this sample has some specific features in magnetic fields of 6–10 kOe.

The magnetic resonance and antiresonance spectra can be reconstructed by the field dependences of wave transmission and reflection coefficients. The antiresonance fields in the spectra of sample no. 4 (Co-embedded nanocomposite) reconstructed from the two

dependences are reasonably close to each other. The resonance spectra reconstructed by the transmission and reflection coefficients are not coincident. This fact implies that the positions of maxima and minima on the field dependences of transmission and reflection coefficients not fully correspond to resonance conditions. For reconstructing real resonance and antiresonance spectra, it is recommended to base upon the frequency dependence of absorbed power, reconstructed from data on the transmission and reflection of electromagnetic waves.

The magnetic resonance and antiresonance spectra of a Fe-embedded nanocomposite sample, reconstructed by the transmission and reflection coefficients (Fig. 8b) show different resonance fields at the same frequency, and this difference is many times higher than the experimental error. The magnetic resonance and antiresonance spectra were also reconstructed for the Ni-embedded nanocomposite. The antiresonance spectrum (Fig. 8c) looks abnormally: The antiresonance field decreases with frequency! The positions of extrema on the dependences for transmission and reflection coefficients are not coincident. This is a common feature of many nanocomposites. Therefore, we can conclude that the real resonance and antiresonance positions for the nanocomposites in hand differ from the positions of extrema on the field dependences of transmission and reflection coefficients. The reason for this circumstance lies in the fact that the materials are strongly magnetically inhomogeneous due to different shapes of nanoparticles. Another possible reason may consist in different sizes of nanoparticles. If magnetization depends on particle size, the magnetic resonance line will be broadened, and the resonance position will differ from the positions of wave transmission and reflection minima. For final conclusions concerning this issue, more detailed research on magnetic properties and electron microscopy data are needed.

Let us compare the magnetic resonance and antiresonance spectra for nanocomposites containing particles of one and two metals, for example, Co or Ni and Co + Ni. The resonance field for the Ni + Co nanocomposite is higher (Fig. 9) than for the Ni or Co nanocomposites. In principle, there are two possible reasons for this phenomenon: Either the magnetization of the Co + Ni nanocomposite is lower compared to the nanocomposites containing one metal or this composite has particles with a different shape with a higher demagnetization factor. The magnetic resonance and antiresonance spectra were also reconstructed for the samples containing Ni, Fe, and Ni + Fe nanoparticles. The conclusion proved to be the same as in the previous case.

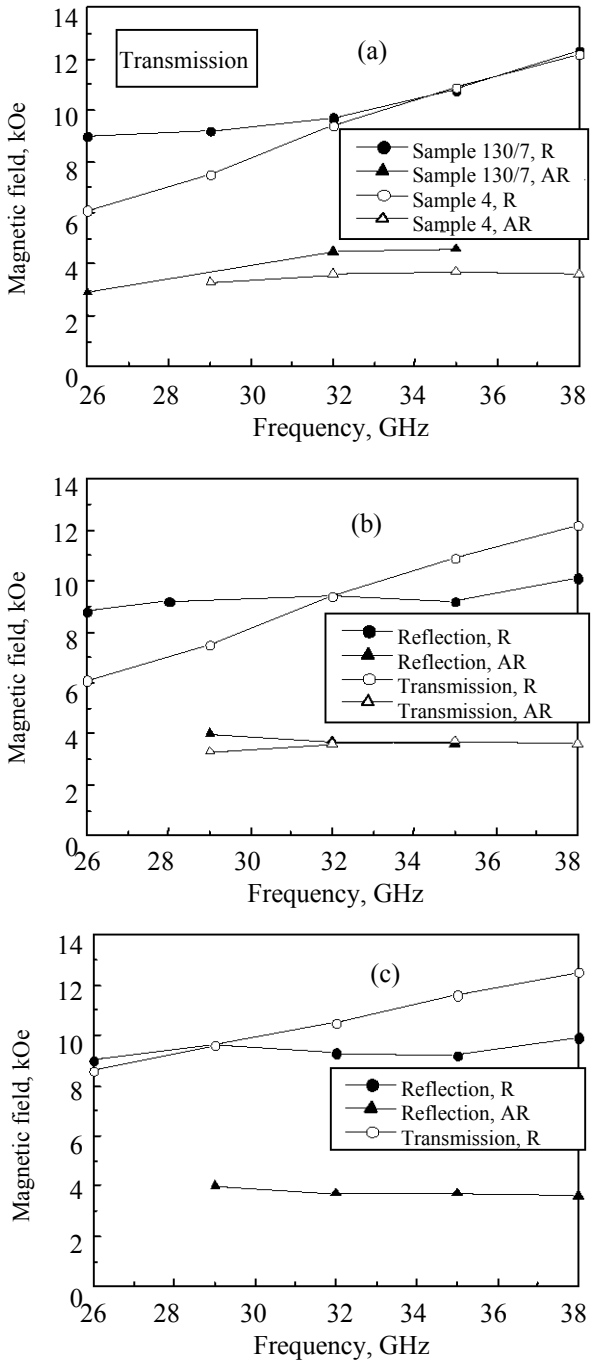

Fig. 8. Magnetic resonance and antiresonance spectra of two 3D nanocomposite samples embedded with (a) cobalt, (b) iron, and (c) nickel nanoparticles: (R) resonance and (AR) antiresonance.

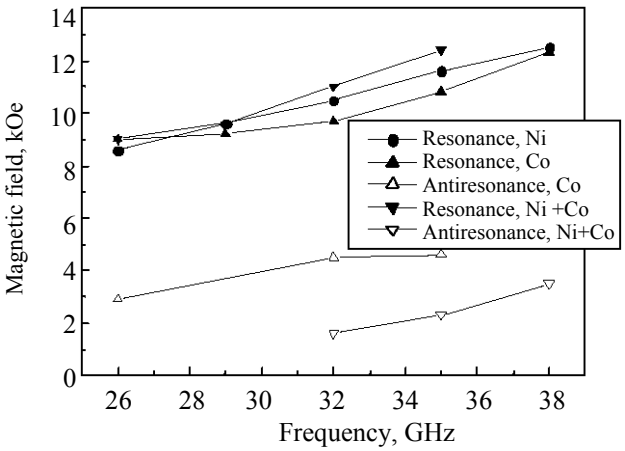

Fig. 9. Magnetic resonance and antiresonance spectra of 3D nanocomposites embedded with cobalt, nickel, and cobalt+nickel nanoparticles.

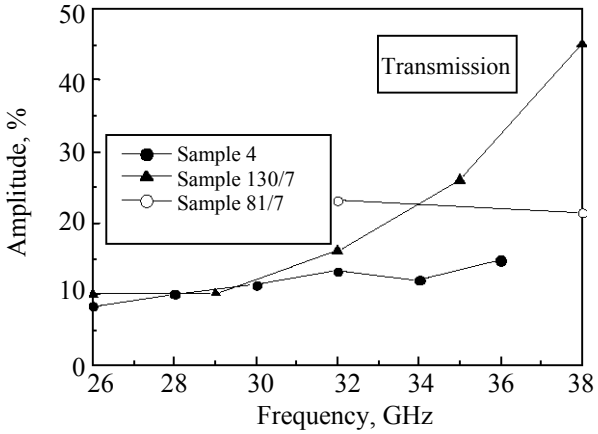

Fig. 10. Frequency dependences of magnetic resonance amplitude for three samples of the cobalt-embedded nanocomposite.

Frequency Dependence of Magnetic Resonance Amplitude

A typical situation in the case of magnetic resonance with a uniform precession mode is that the resonance amplitude increases with frequency. As the frequency increases, the resonance field and precession frequency increase, and the magnetic moment has enough time to fulfill a greater number of spins. This enhances the efficiency of the magnetic moment–wave interaction and, as a result, increases the resonance amplitude.

Let us consider in more detail the changes in the magnetic resonance and antiresonance amplitudes for the nanocomposites in hand. The field dependences of resonance amplitude, measured by the transmission coefficients for three samples of the cobalt-embedded nanocomposite (Fig. 10), are quite different from each other, which depends on such engineering factors as impregnation and crystallization temperatures. An increase of amplitude with frequency is observed for two samples and is not observed for sample no. 81/7 (measurements at only two frequencies are available for this sample). A fairly sharp increase of resonance amplitude is observed for sample no. 130/7. The resonance amplitude is more than 40%, which is of interest for technical applications.

Let us consider the frequency dependences of the resonance amplitudes measured for the same sample by the field dependences of transmission and reflection

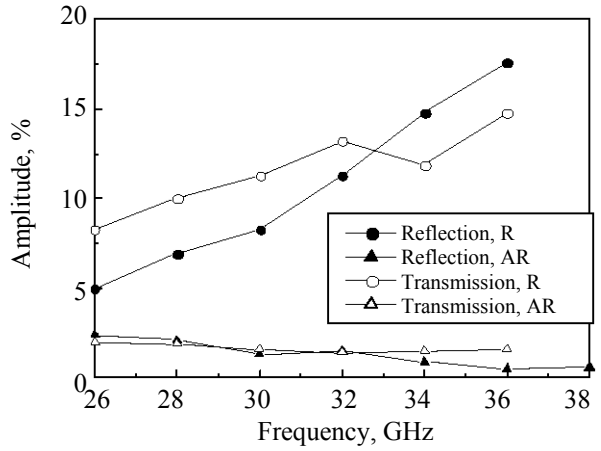

Fig. 11. Frequency dependence of the amplitude of resonance and antiresonance in wave transmission and reaflection for the cobalt-embedded nanocomposite: (R) resonance and (AR) antiresonance.

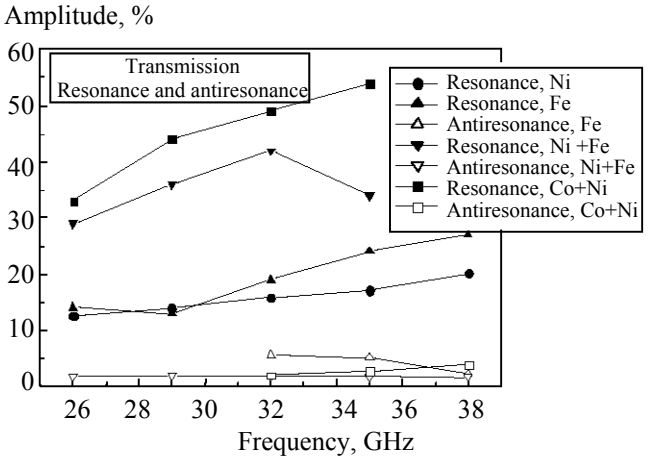

Fig. 12. Frequency dependence of the resonance and antiresonance amplitudes in the samples embedded with particles of one metal (Ni or Fe) and two metals (Ni + Fe or Co + Ni).

coefficients. Naturally, the resonance amplitudes in wave transmission and reflection should not coincide.

It is seen in the spectrum obtained for the Co-embedded nanocomposite (Fig. 11) that the resonance amplitude increases with frequency by the results of measurements of both transmission and reflection coefficients. The frequency dependence of anti-resonance amplitude is unusual: The amplitude decreases as the frequency increases. The frequency dependence of antiresonance amplitude for the Ni-embedded nanocomposite is similar.

Figure 12 compares the frequency dependences of resonance and antiresonance amplitudes, obtained for 3D nanocomposites containing particles of one metal (Ni, Fe, Co) and two metals (Ni + Fe, Co + Ni). As seen, the resonance amplitudes of two metal-embedded nanocomposites are much higher than those of one metal-embedded nanocomposites. This observable may entail important consequences in terms of technical applications of materials of this class.

The presented results of research on metal-containing nanocomposites on the basis of opal matrices create prerequisites for the development of high-frequency devices controlled by magnetic field, whose functioning is underlain by microwave magnetic resonance in such nanocomposite materials. These materials can find application in controlled attenuators, phase inverters, and other millimeter-range devices.

ACKNOWLEDGMENTS

The work was financially supported in part by the Russian Academy of Sciences in the framework of the "Basic Research in Nanotechnologies and Nanomaterials" Program (project no. NSh-6172.2012.2) and by the Ministry of Education and Science of the Russian Federation in the framework of the State Contract 2.5737.2011 "Electromagnetic Properties of Metal and Composite Nanostructured Materials in the Millimeter Wavelength Range".

The authors are grateful to V.G. Pushin, V.S. Gaviko, and A.V. Korolev for electron microscopy and magnetic measurements at the Center for Collective Use, Institute of Metal Physics, Ural Branch, Russian Academy of Sciences.

REFERENCES

1. Ozbay, E., Temelkuran, B., and Bayindir, M., *Prog. Electromagn. Res*., 2003, vol. 41, pp. 185–209.
2. Sarychev, A.K. and Shalaev, V.M., *Electrodynamics of Metamaterials,* Singapore: World Scientific, 2007.
3. *Photonic Glasses*, Fuxi Gan and Lei Xu, Eds., London: Imperial College Press, 2006.
4. *Silicon Photonics*, Pavesi, L. and Lockwood, D.J., Eds., *Top. Appl. Phys*., 2004, vol. 94.
5. Cole, R.M., Sugawara, Y., Baumberg, J.J., Mahajan, S., Abdelsalam, M., and Bartlett, P.N., *Phys. Rev. Lett*., 2006, vol. 97, p. 137401.
6. Astrova, E.V., Borovinskaya, T.N., Tolmachev, V.A., and Perova, T.S., *Fiz. Tekh. Poluprovodn*., 2004, vol. 38, no. 9, pp. 1125–1128.
7. Samoilovich, M.I., Belyanin, A.F., Yurasov, N.I., Kleshcheva, S.M., Tsvetkov, M.Yu., Gan'shina, E.A., Perov, N.S., Agafonov, S.S., Glazkov, V.P., Sanenkov, V.A., and Cherepanov, V.M., Abstracts of Papers, *XII Mezhdunarodnaya nauchno-tekhnicheskaya konferentsiya "Vysokie tekhnologii v promyshlennosti Rossii (Materialy i ustroistva funktsional'noi elektroniki i mikrofotoniki)"* (Proc. XII Int. Scientific and Technical Conf. "High Technologies in Russian Industry (Materials and Devices of Functional Electronics and Microphotonics)", Moscow, 2006, pp. 32–39.
8. Richard, W., *Phys. Rev. E*, 2001, vol. 64, p. 056625.
9. Kong, J.A., *Prog. Electromagn. Res*., 2002, vol. 35, pp. 1–52.
10. Efros, A., Shi Jing, Blair, S., DeLong, M., and Vardeny, Z.V., *Proc. NSF Nanoscale Science and Engineering Grantees Conf*., Arlington, VA, December 11–13, 2002.
11. Usadel, K.D., Phys. Rev. B, 2006, vol. 73, p. 212405.
12. Pimenov, A., Loidl, A., Przyslupski, P., and Dabrowski, B., *Phys. Rev. Lett*., 2005, vol. 95, p. 247009.
13. Silveirinha, M.G. and Engheta, N., *Phys. Rev. Lett*., 2006, vol. 97, p. 157403.
14. Edwards, B., Alu, A., Young, M., Silveirinha, M., and Engheta, N., *Phys. Rev. Lett*., 2008, vol. 100, p. 033903.
15. Ziolkowski, R.W., *Phys. Rev. E*, 2004, vol. 70, no. 4, p. 046608.
16. Buchanan, K.S., Zhu, X., Meldrum, A., and Freeman, M.R., *Nano Lett*., 2005, vol. 5, no. 2, pp. 383–387.
17. Moiseev, S.G., Pashinina, E.A., and Sukhov, S.V., *Kvant. Elektron*., 2007, vol. 37, no. 5, pp. 446–452.
18. Usadel, K.D., *Phys. Rev. B*, 2006, vol. 73, p. 212405.
19. Alves, C.R., Aquino, R., Depeyrot, J., Tourinho, F.A., Dubois, E., and Perzynski, R., *Proc. 4th Brazilian MRS Meeting*, Gramado-RS, February 25–29, 2007.
20. Su, H., Zhang, H., Tang, X., and Liu, Y., *J. Mater. Sci*., 2007, vol. 42, pp.2849–2853A.
21. Rinkevich, A.B., Perov, D.V., Burkhanov, A.M., Samoilovich, M.I., Kleshcheva, S.M., and Kuznetsov, E.A., Abstract of Papers, *XVI Mezhdunarodnaya nauchno-tekhnicheskaya konferentsiya "Vysokie tekhnologii v*

promyshlennosti Rossii (Materialy i ustroistva funktsional'noi elektroniki i mikrofotoniki)" (Proc. XVI Int. Scientific and Technical Conf. "High Technologies in Russian Industry (Materials and Devices of Functional Electronics and Microphotonics)", Moscow, 2010, pp. 59–65.

22. Rinkevich, A.B., Ustinov, V.V., Samoilovich, M.I., Kleshcheva, S.M., and Kuznetsov, E.A., Abstracts of papers, *XIII Mezhdunarodnaya nauchno-tekhnicheskaya konferentsiya "Vysokie tekhnologii v promyshlennosti Rossii (Materialy i ustroistva funktsional'noi elektroniki i mikrofotoniki)"* (Proc. XIII Int. Scientific and Technical Conf. "High Technologies in Russian Industry (Materials and Devices of Functional Electronics and Microphotonics)", Moscow, 2007, pp. 77–87.